ЖЭТФ, 2015, том 147, вып. 6, стр. 1230–1243

TUNNELING SPECTROSCOPY OF A PHOSPHORUS IMPURITY ATOM ON THE Ge(111)-(2 × 1) SURFACE

S. V. Savinov [a], **A. I. Oreshkin** [a*], **S. I. Oreshkin** [b], **C. van Haesendonck** [c]

[a] *Lomonosov Moscow State University*
119991, Moscow, Russia

[b] *Sternberg Astronomical Institute, Lomonosov Moscow State University*
119991, Moscow, Russia

[c] *Laboratorium voor Stoffysica en Magnetisme*
B3001, Heverlee, Belgium

Received October 7, 2014

We numerically model the Ge(111)-(2 × 1) surface electronic properties in the vicinity of a P donor impurity atom located near the surface. We find a notable increase in the surface local density of states (LDOS) around the surface dopant near the bottom of the empty surface state band π^*, which we call a split state due to its limited spatial extent and energetic position inside the band gap. We show that despite the well-established bulk donor impurity energy level position at the very bottom of the conduction band, a surface donor impurity on the Ge(111)-(2 × 1) surface might produce an energy level below the Fermi energy, depending on the impurity atom local environment. It is demonstrated that the impurity located in subsurface atomic layers is visible in a scanning tunneling microscope (STM) experiment on the Ge(111)-(2 × 1) surface. The quasi-1D character of the impurity image, observed in STM experiments, is confirmed by our computer simulations with a note that a few π-bonded dimer rows may be affected by the presence of the impurity atom. We elaborate a model that allows classifying atoms on the experimental low-temperature STM image. We show the presence of spatial oscillations of the LDOS by the density-functional theory method.

DOI: 10.7868/S0044451015060178

1. INTRODUCTION

At present, it is a common place that the Ge(111)-(2 × 1) surface consists of π-bonded zigzag chains. This was confirmed many times by different means (see [1–3] and the references therein). Surprisingly, just a few publications are devoted to investigations of impurity atoms on the (111) surface of elemental semiconductors [4–11]. And as one can see, the interest in the Si(111)-(2 × 1) surface is renewed. But not the interest in the Ge(111)-(2 × 1) surface. This is unexplainable, because Ge is the main candidate for technology to overcome scaling limits of Si-based MOSFETs [12]. The knowledge of local properties of Ge, especially of those caused by impurity atoms, is of vital importance. Besides, the surface and interface properties of Ge(111) have great significance for Ge spintronics applications. It is known that Ge has some advantages compared with Si [13]. The scanning tunneling microscopy (STM) method is currently the only physical method achieving atomic resolution in real space. But experimenters often suffer from the lack of some reference points provided by the theory. For example, reliable STM image interpretation still remains a challenging task. There is no general approach taking all kinds of physical processes responsible for the STM image formation into account. Below, we report on a surface electronic structure investigation performed by *ab initio* computer simulations in the density functional framework, which is a first-order estimation for STM/STS (scanning tunneling spectroscopy) images and can serve as a basis for further model improvements. We restrict the present investigation to the case of left (negative) only surface buckling (Fig. 1*a*) because this matter is still controversial and is the subject of intensive investigations [14–16]. Our research is in some sense similar to the one reported in [4] for the Si(111)-(2 × 1)

*E-mail: oreshkin@spmlab.phys.msu.su, oreshkin@spmlab.su

surface. But in reconstructing two surface bi-layers of Ge(111)-(2 × 1) we take all possible impurity positions into account, and besides, our analysis is not aimed at a pure STM image simulation, but rather at comprehensive analysis of the local density of states.

2. METHODS

We have performed our density-functional theory (DFT) calculations in the local-density approximation (LDA) as implemented in the SIESTA package [17]. The use of strictly localized numerical atomic orbitals is necessary in order to finish the modeling of a large surface cell in reasonable time. The surface Ge(111)-(2 × 1) supercell consists of 7 × 21 cells of elementary 2 × 1 reconstruction, each 8 Ge atomic layers thick (the total of 2646 atoms). The vacuum gap is chosen rather big, about 20 Å. The Ge dangling bonds at the slab bottom surface are terminated with H atoms to prevent surface state formation. The geometry of the structure was fully relaxed until atomic forces have became less than 0.003 eV/Å. More details about the calculations can be found elsewhere [18]. As we have reported earlier, the atomic structure of the Ge(111)-(2 × 1) surface is strongly disturbed in the vicinity of surface defects [18, 19]. A few π-bonded rows around the defect are affected. That is why the geometry relaxation has been performed with a large supercell to keep the internally periodic DFT images of impurity well separated. However, this is still an open question if the separation of defect images is sufficiently large. At the last step of simulation, the spatial distribution of Khon–Sham wave functions and the corresponding scalar field of the surface electronic local density of states LDOS(x, y, eV) were calculated. Because of the strictly localized atomic orbitals used in SIESTA, the special procedure of wave-function extrapolation into the vacuum has to be used (it is also implemented in the SIESTA package).

3. RESULTS

3.1. Geometry and ground-state properties

In the STM method, the LDOS is measured above the surface. The tails of wave functions actually make the image. Hence, in DFT calculations we are interested in the quantity

$$\mathrm{LDOS}(x, y, eV) \sim \sum_i |\Psi_i(x, y)|^2 \widetilde{\delta}(E - E_i)|_{z=\mathrm{const}},$$

where Ψ are Khon–Sharm eigenfunctions, $\widetilde{\delta}$ is a finite-width smearing function, E_i are Khon–Sham eigenvalues, and summing is evaluated in a certain plane ($z = \mathrm{const}$) located a few angstroms above the surface. Here, the broadening is an essential part of calculations, because we know from our experience that tunneling broadening in STM experiments on semiconductors typically amounts to about 100 meV. The broadening provides the degree of LDOS smoothing necessary to resemble experimental tunneling spectra. At the first stage of DFT calculations, the equilibrium geometry has to be established in the reconstruction of a unit cell of Ge(111)-(2 × 1). Afterwards, the unit cell is enlarged to the desired extent, the defect is introduced, and the structure is relaxed again. The final step is the LDOS(x, y, eV) calculation. The results are sketched in Fig. 1.

Figure 1*b* illustrates the electronic structure of a clean Ge(111)-(2 × 1) surface. Two surface state (SS) bands, empty (π^*) and filled (π), can be seen in the projected band gap. The widths of SS bands derived from Fig. 1*b* are $\Delta\pi^* = 1.24$ eV and $\Delta\pi = 0.44$ eV. The surface band gap ΔE_{sbg} is about 0.3 eV. As should be expected, the LDA gives the band gap value that is much smaller than the experimental one. SS bands, as well as bulk bands, are also shown in Fig. 1*b* by small grey rectangles next to the ordinate axis. This representation is used in the majority of figures below. The surface band structure is presented for the Ge(111)-(2 × 1) surface with negative buckling. Our calculations predict that the negative surface isomer is energetically (by almost 11 meV per (2 × 1) unit cell) more favorable and, as we stated above, we restrict the present analyses to the negative buckling only. Jumping ahead, we display the LDOS(eV) curve in Fig. 1*c*. The calculated $I(V)$ dependence on a logarithmic scale is also shown. The surface LDOS(eV) curve is the result of averaging over the whole 8 × 5 nm^2 area in Fig. 1*a*. The gap right below the Fermi level is clearly observed on the LDOS(eV) graph. It does not correspond to the bulk band gap. The closest resemblance can be found with the surface band gap. Rectangles at the absissa axis in Fig. 1*c* illustrate energy positions of different bands. Everywhere below, the bottom of the conduction band is schematically shown on the figures for the case of the Ge(111)-(2 × 1) surface at room temperature. In this case, the optical band gap is about 0.5 eV [20].

To give a clear impression of the relation between the surface band structure and the LDOS, the latter is also depicted on the left of the surface band diagram in Fig. 1*b*. Besides a complicated band diagram on the surface, bands are bent near the surface due to charge accumulation on SSs. This is illustrated in Fig. 1*d*. Thus, there are two points of complication for tunneling into the Ge(111)-(2 × 1) surface. First, the

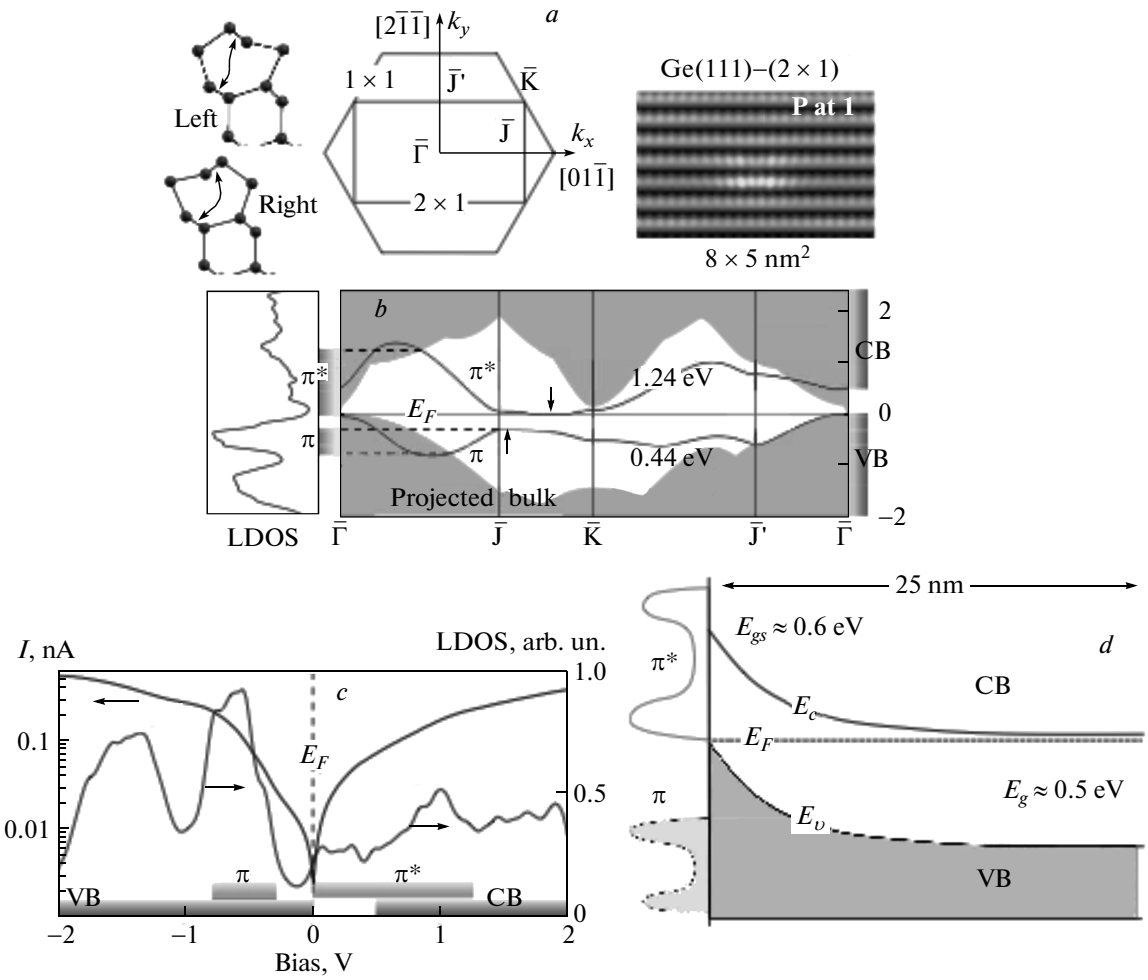

Fig. 1. (a) Sketches of left and right isomers of the Ge(111)-(2 × 1) surface. Two bonds, appropriate for definition, are marked by arrows. The irreducible Brilloin zones for Ge(111)-(1 × 1) and Ge(111)-(2 × 1) surfaces together with special points and relevant directions are shown. The model surface slab with an impurity atom positioned at site 1 is correctly oriented with respect to crystallographic directions. (b) Surface band diagram for Ge(111)-(2 × 1) reconstruction. The empty (π^*) and filled (π) surface-state bands can be seen in the projected band gap. Their energetic position is schematically shown at the ordinate axis by grey rectangles. To illustrate the relation between the surface band structure and the LDOS(eV), the latter is shown in the left pane. The π^* bottom and the π top are marked by arrows. The bulk band energetic position is shown on the right. (c) The LDOS(eV) curve and the $I(V)$ curve on a logarithmic scale, averaged above the whole 8×5 nm^2 surface slab shown in Fig. 1a. (d) Surface band structure in energy-space coordinates. A space gap between the surface and bulk states is visible; E_{gs} is the surface band gap, E_g is the bulk band gap

minimum and maximum of SSs are located near the $\bar{J}$ point (Fig. 1b), while STM experiment emphasizes the $\bar{\Gamma}$ point. Second, there exists a spatial gap between surface and bulk states at small bias voltage (Fig. 1c). The STM experiment on Ge(111)-(2 × 1) surface involves many different processes.

3.2. LDOS scalar field representation

In the exposition in what follows, we focus mostly on the LDOS properties, and before we go to the main results, we have to clarify the physical meaning of our data representation for the LDOS. Below, we speak about cross-sectioning of the LDOS(x, y, eV) scalar field (Fig. 2a). The x and y directions correspond to [01$\bar{1}$] and [2$\bar{1}\bar{1}$] crystallographic directions. The two most relevant quantities are cross sections of the scalar field LDOS(x, y, eV) in the x, y and x, eV planes, LDOS(x, y) and LDOS(x, eV). The LDOS is built for different impurity atom positions in two subsurface bilayers of the Ge(111)-(2 × 1) reconstruction.

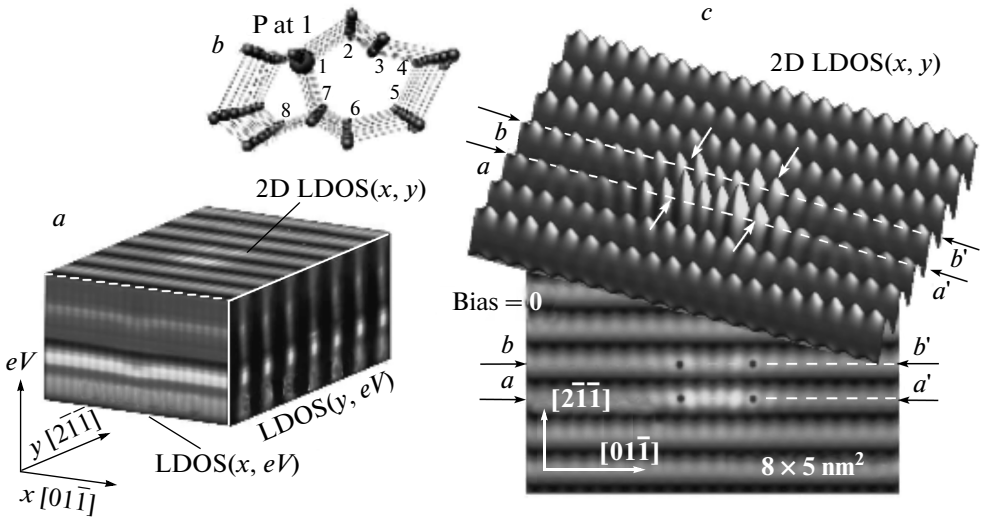

Fig. 2. (a) Sketch LDOS(x, y, eV) scalar field. Relevant directions are shown. (b) Labels to identify the donor atom position in two surface bilayers of Ge(111)-(2 × 1) reconstruction. The P atom is shown in position 1. (c) Quasi-3D and 2D representations of the LDOS$(x, y)_{|eV=0}$ cross section of the LDOS(x, y, eV) scalar field at zero bias. Specific points and directions are indicated

The definition of our notation for the donor atom position is presented in Fig. 2b. Worthy of note, the impurity atom does not exactly occupy the same lattice site as the host atom it substitutes. In Fig. 2c, we show the cross sections LDOS$(x, y)|_{eV=0}$ at a fixed bias voltage for a P donor atom located at position 1 in the surface bilayer. These images roughly correspond to experimental STM images, because at small bias voltage there are not too many sharp LDOS features contributing to the image. It can be seen from Fig. 2 that two π-bonded rows of surface reconstruction are influenced by the impurity. In each row, a protrusion can be observed. The spatial extent of the impurity-induced feature along the direction of the π-bonded dimer row ([01$\bar{1}$] direction) is at least 40 Å. We note two distinguishable maxima on the protrusion. We return to this fact later. Arrows and dots on the image, as well as a–a' and b–b' lines, mark spatial points and directions referred to in the figures below.

3.2.1. Split state

We have found a notable increase in the LDOS in the vicinity of an impurity atom at the bottom of the empty SS band π^*. We refer to it as a split state. Figure 3 proves the validity of this terminology. In the figure, the LDOS(x, y, eV) field is shown by surfaces of equal value, colored by the applied tunneling bias voltage. The LDOS is drawn for two π-bonded rows denoted as a–a' and b–b' in Fig. 3. The donor atom position is depicted in the figure. To prevent the confusion caused by a quasi-3D picture, we clarify that the impurity is located on the left side for the π-bonded row b–b', and on the right side for the π-bonded row a–a'. We note some important facts about this LDOS representation. First of all, high LDOS values are confined within areas bounded by a constant-value surface. They are perfectly localized above the π-bonded rows. This is the reason why only every second dimer row is imaged by STM. In between the π-bonded rows, the LDOS is relatively low. Beside, all round-shaped vertical structures in the π-bonded row are located above the up-atom. The down-atom can be found in between them. Such a spatial structure of the LDOS is a consequence of the collective π-bond formation. STM can only image the up-row dimers, and therefore, only up-rows. Basically, with the used approach, the π-bonds can also be directly visualized [18]. The hybridization of atomic orbitals is clearly visible from Fig. 3. It is very strong in the close proximity of a surface defect. This causes the appearance of a specific feature near the bottom of the empty SS band (marked by arrows in Fig. 2). The limited spatial and energy extents of this feature as well as its position in the band gap imply that this is indeed a split state. We are working with the microscopic picture, on the level of individual atoms. That is why we are able to see the connection between atomic orbital hybridization and the macroscopic band structure. Surface states appear due to atomic arrangement of the surface. Split states appear

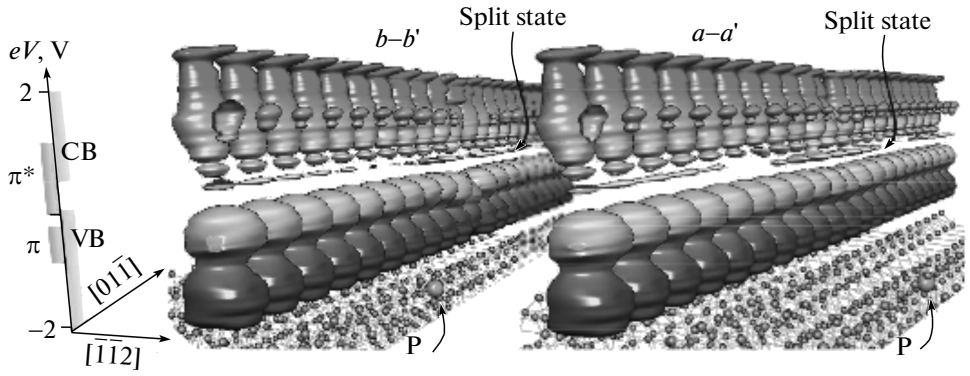

Fig. 3. LDOS(x, y, eV) field above rows a–a' and b–b' (see Fig. 2) shown by constant-value surfaces. Coloring corresponds to the applied bias voltage. The split state in the band gap can be clearly observed above both dimer rows. Note the changes of structure at the right of the CB features and strong hybridization of atomic orbitals around the impurity atom

due to changes in this arrangement around the defect. They both have the same root: hybridization of atomic orbitals. One problem exists. It is difficult to define the energetic position reference level: is it the Fermi energy or the SS π^*-band bottom? To be accurate, we refer to the Fermi level, i. e., the split state is located at the Fermi level, and not near the π^* bottom.

3.2.2. Energy profiles

Important for understanding our results are the cross sections LDOS$(x, eV)|_{a-a'(b-b')}$ at a fixed y coordinate, which are shown in Fig. 4. They are taken along (a–a') and (b–b') planes in Fig. 2, i. e., along π-bonded rows of Ge(111)-(2 × 1) reconstruction. Areas near the Fermi level, where a split state resides, are zoomed in on the insets. The positions of the Fermi level E_F, the conduction band (CB) bottom, the valence band (VB) top, and the empty π^* and filled π SS bands are indicated in Fig. 3. According to our DFT calculations, the VB top almost coincides with the bottom of the empty SS band π^* and the Fermi level (see Fig. 1 and Ref. [18]). Even more, the π^* band can be partially filled at a very high doping ratio [21]. For a Ge(111)-(2 × 1) surface with negative buckling, our calculations also predict the position of the empty SS π^* band bottom about tens of meV below the Fermi level. The proportions of LDOS(x, eV) images are chosen on purpose in a way that is convenient for experimenters. Typically, the number of points along the spatial direction is less than the number of bias voltage points, and the tunneling spectra image is elongated in the vertical direction. Although the DFT band gap in the LDA is nonphysically small, it is also shown in Fig. 4*a* for completeness. The distribution LDOS(x, eV) is reach in features. Its cross section along the x coordinate gives the LDOS(x) profile exactly in the same way as does the cross-sectioning of LDOS(x, y) (see Fig. 1) along the x coordinate.

The cross sections of (a–a') and (b–b') planes along the c–c' line are shown in Fig. 4*b*. We can see two distinct maxima on the profiles. Importantly, the spatial extent of perturbation is obviously about 80 Å. The 40 Å estimation from Fig. 2 suffers from unsufficient contrast of the LDOS$(x, y)|_{eV=0}$ image. The cross section of LDOS(x, eV) along the eV coordinate (d–d', e–e', f–f', and g–g' lines in Fig. 4*a*) corresponds to point spectroscopy LDOS(eV) dependences (Fig. 4*c*) at the LDOS(x) profile points marked by vertical arrows in Fig. 4*b*. These are points shown in Fig. 2 by dots and arrows. The curves d–d' and f–f' are taken between dimers in the π-bonded row, while the curves e–e' and g–g' are taken on top of dimers (see Figs. 2 and 4*b*). Minima and maxima refer to the bias voltage equal to −0.5 V. For the whole range of bias voltage, the LDOS values collected between dimers are higher than the value on top of dimers, except for a narrow interval in the vicinity of the Fermi energy, where the split state resides. This split state contributes to the increase in the LDOS on top of dimers in the π-bonded row. Hence, the protrusion consisting of a few dimers appear on the LDOS(x, y) (as well as on STM) image. It follows from Fig. 4*c* that the contrast of protrusion is higher on the (a–a') plane than on the (b–b') plane, and this indeed can be observed in Fig. 2.

3.2.3. Spatial profiles

In Fig. 5, to illustrate the usefulness of the LDOS(x, eV) map, we show a set of cross sections along the spatial coordinate for a P donor atom located at

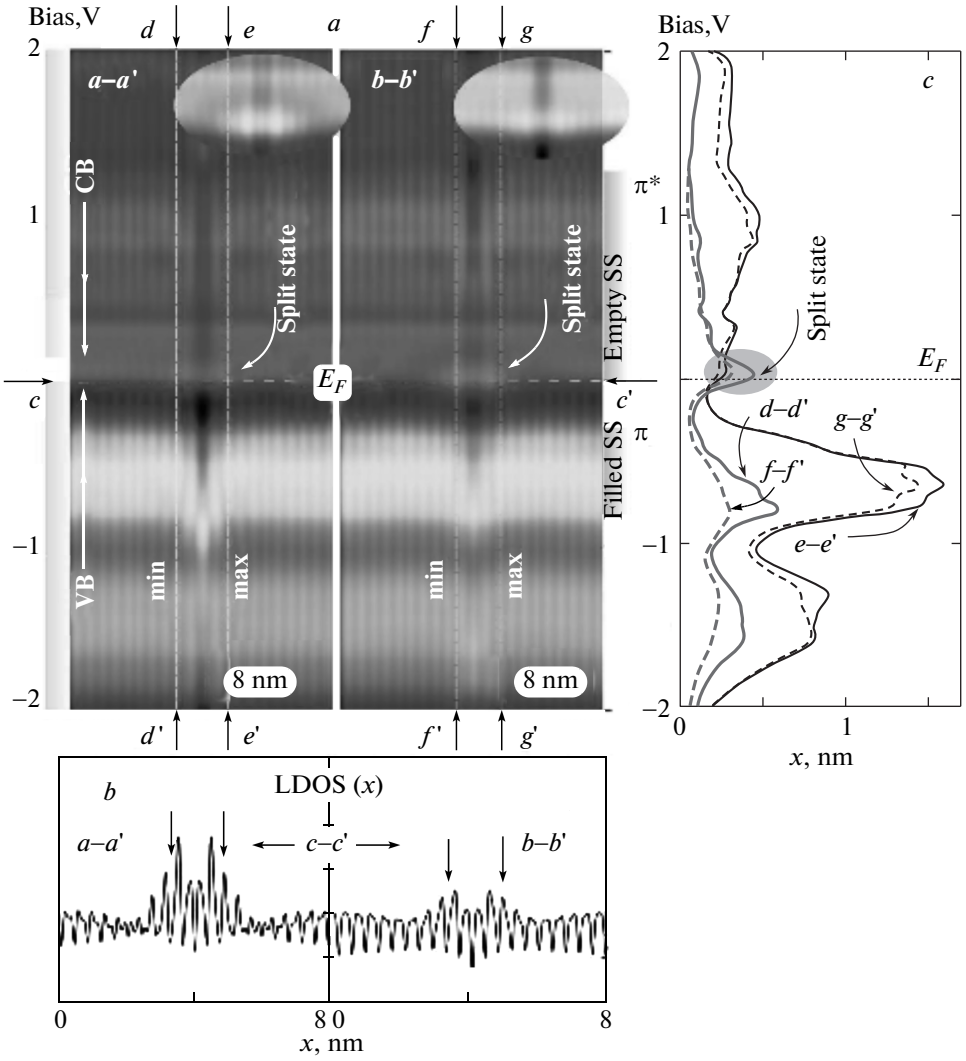

Fig. 4. (*a*) 2D LDOS(x, eV) distributions taken along a–a' and b–b' planes in Fig. 2. The impurity atom is at 1 site. Two rectangles at the left side correspond to optical and DFT conduction band positions. (*b*) Profiles of (a–a') and (b–b') planes along the c–c' line, which are essentially the same as profiles of images in Fig. 2 along a–a' and b–b' lines. (*c*) Profiles of a–a' and b–b' images along d–d', e–e', f–f', and g–g' lines, which are LDOS(eV) dependences at the points shown in Fig. 2 by black dots and white arrows. Axis directions and image size are indicated

position 1. The profiles are slightly low-pass filtered to stress the long-range features, and they therefore look somewhat different compared to Fig. 4*b*. When the tunneling bias changes, the LDOS(x) profile also changes, revealing depressions and protrusions of different shapes. The profile corresponding to the split-state energy (and to the presence of a protrusion on the STM image) is marked by a grey ellipse. We can easily see that the protrusion amplitude at the Fermi level is much less than the amplitude of features at other bias voltages (see also Fig. 4*c*). We also note that the impurity LDOS image might have an elongated hillock-like shape at positive bias (empty states). This means that the protrusion on the LDOS image is not caused by charge density effects (like charge screening). To the best of our knowledge, this fact was never clearly stated. In other words, the STM image of the Ge(111)-(2 × 1) surface [8] (as well as the Si(111)-(2×1) surface [4–6]) around a surface defect is dominated by the split state in the vicinity of the Fermi level, although the amplitude of the effect is relatively small.

3.2.4. Quasi-3D representation

To give even more insight into the power of the LDOS(x, eV) data representation, it is drawn as a qua-

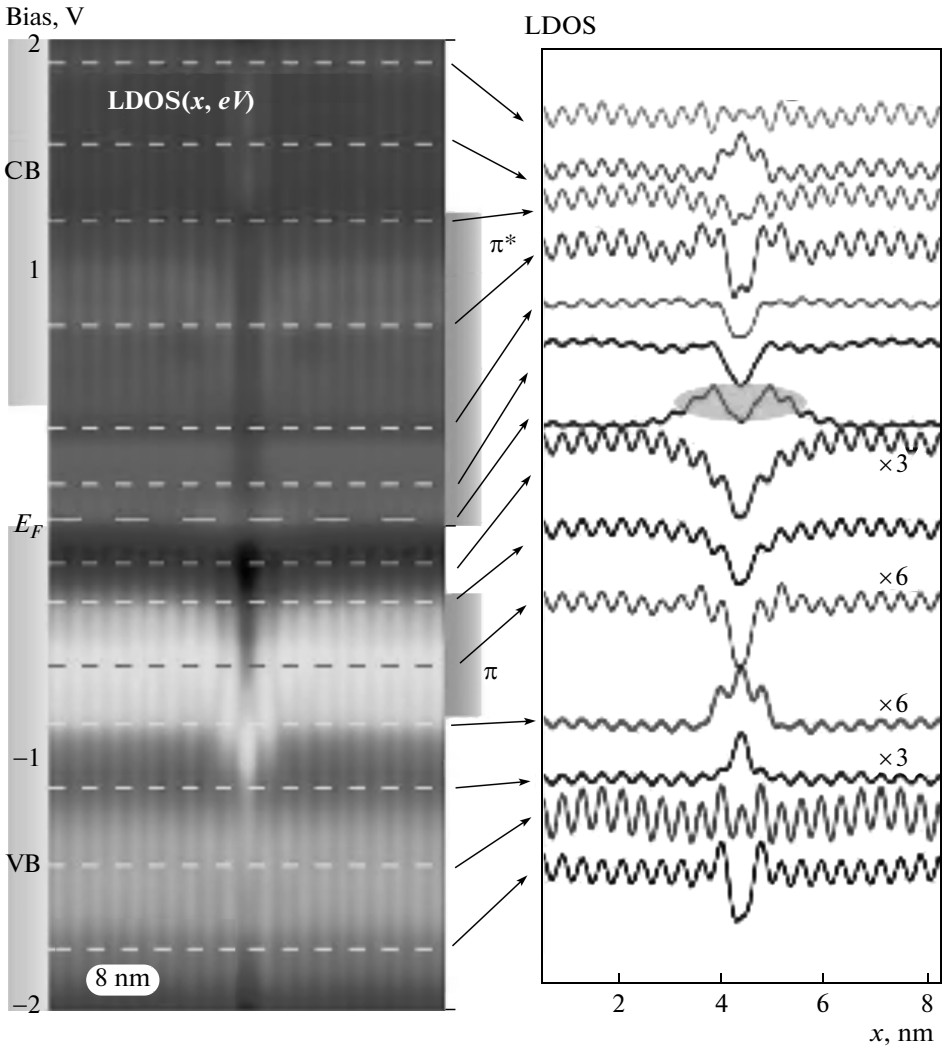

Fig. 5. LDOS(x, eV) map along the b–b' dimer row in the vicinity of the P atom, located at position 1 on the Ge(111)-(2×1) surface and its cross sections along the indicated lines

si-3D surface in Fig. 6. Height is given on a logarithmic scale to increase the image height contrast. The LDOS value is encoded both by height and by color. The spatial and energetic positions of specific features of the tunneling spectrum can be easily deduced from the figure. The split state (zoomed in on the inset) is located at the Fermi level. It has a cigar-like spatial shape, which is directly reflected in the shape of the protrusion on the LDOS(x, y) image. It is also obvious from Fig. 6 that the split state actually fills the whole width of the LDOS(x, eV) spectrum. Hence, we cannot completely exclude the possibility of an overlap of impurity-induced electronic features between neighboring supercells of calculation. This overlap can introduce some difficulty in estimating errors in quantum mechanical evaluation of forces. This is the main reason why we have increased the size of the geometry relaxation surface cell to the upper available to its limit. We now finish the overview of data representation. Taking the foregoing into account, we can conclude that, given LDOS(x, eV), it is readily possible to estimate the outlook of point spectroscopy curves as well as the shape of spatial profiles. That is why the results of calculations of electronic properties for all 8 possible positions of the P impurity atom in two surface bilayers (see Fig. 2) are presented below in Fig. 8 as LDOS(x, eV) maps.

3.3. Local tunneling spectroscopy

Another problem we would like to discuss is the local spectroscopy LDOS(eV) curves. This article is written with experimental needs in mind, and we therefore

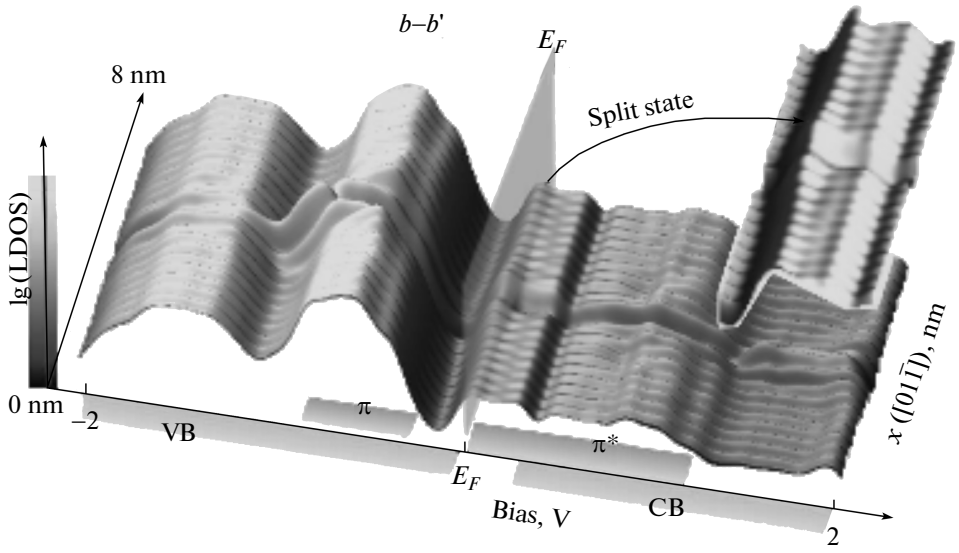

Fig. 6. Quasi-3D representation of LDOS(x, eV) along the b–b' π-bonded row in Fig. 2. The area containing the split state is zoomed in to give a clear impression about its spatial structure. The Fermi level is shown as a semitransparent plane. The LDOS values are given on a logarithmic scale to increase the height contrast. The LDOS values are encoded both by height and by color

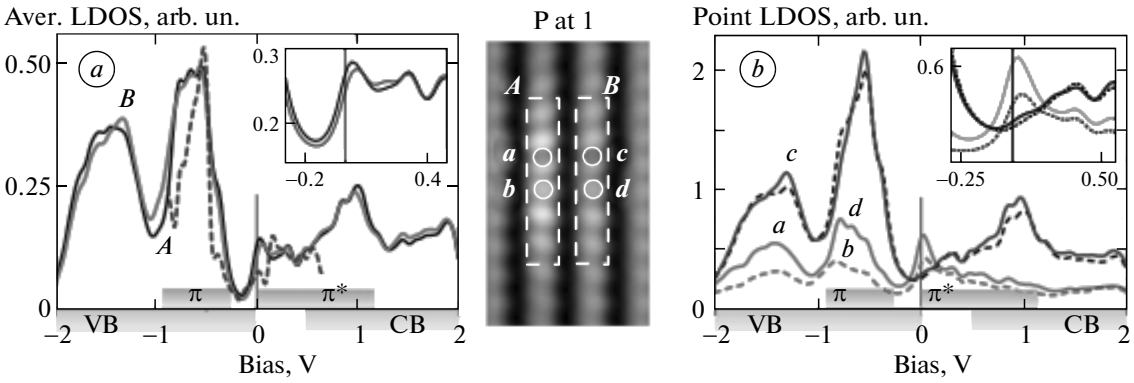

Fig. 7. Theoretical tunneling spectra obtained (a) by averaging over A and B areas and (b) by point measurement at a, b, c, and d points. The dashed line on the left plane is the experimental tunneling spectrum. Insets depict the zoomed in part of LDOS(eV) curves around the Fermi energy. The middle part sketches the surface area above which the spectroscopy was performed. Areas A and B are respectively located above the a–a' and b–b' π-bonded dimer rows (see Fig. 2). Points b and d are located on the top of dimers in a row, while points a and c lie between the dimers. The band structure is shown on the abscissa axis

analyze spectroscopy curves as if they were obtained by STM. There are two approaches to measure the tunneling spectra. One is the simple $I(V)$ curve measurement at a certain surface point. It heavily relies on a very high stability of the mechanical system. Basically, this is the case in recent years. Another approach is based on averaging the $I(V)$ curves above some surface area. It is less sensitive to different noise. The problem is that the two approaches can give results that are different at first glance. In Fig. 7, we present model tunneling spectra for different measurement conditions for a P atom located at site 1. In Fig. 7a, there are spectra averaged over A and B areas above π-bonded rows. In Fig. 7b, spectroscopy curves at points a, b, c, and d are depicted. Points b and d are located on the top of dimers in a row. Points a and c are between the

dimers. Curves A and B are almost indistinguishable, although the heights of protrusions along a–a' and b–b' lines (see also Fig. 2) on the LDOS(x, y) image strongly differ. The split state is located close to the Fermi level, and this part of the spectrum is zoomed in on the inset. The difference in the averaged spectra is on a few percent scale, which apparently is not enough to draw any reliable conclusions. We note a nonzero tunneling conductivity at the Fermi energy. The dashed line in Fig. 7*a* corresponds to experimental tunneling spectroscopy data.

We can see a reasonably good agreement between theory and experiment. The data was obtained by averaging over a relatively small surface area, and hence it looks more similar to point spectroscopy.

As to point spectroscopy, we can easily discriminate atomic-size features. Dimers at similar positions in different dimer rows give different tunneling spectra (Fig. 7*b*). Even the relatively small difference above the elevated features along dimer rows is obvious. Looking at the spectra obtained by different methods, we can conclude that point spectroscopy does not give immediate impression of the band structure, while spectroscopy with averaging does. Averaging two point spectroscopy curves, one on top of the dimer and the other in between dimers, gives a curve similar to the averaged spectroscopy curve. We also note the vertical scales on both panels. The averaging significantly decreases the maximum value. There are no obvious specific points on the numerical tunneling conductivity $I(V)$ dependence (nor on its derivative) allowing simple determination of band gap edges (see Fig. 1). In other words, having perfectly defined $I(V)$ and knowing the LDOS, we cannot determine the band gap, although this can be caused by the very narrow DFT band gap. Another conclusion that can drawn from local spectroscopy analysis is that it is almost impossible to identify an individual impurity on the Ge(111)-(2×1) surface relying only on the results of local spectroscopy. As we discussed earlier, the LDOS maps should be used together with local spectroscopy data [18, 22].

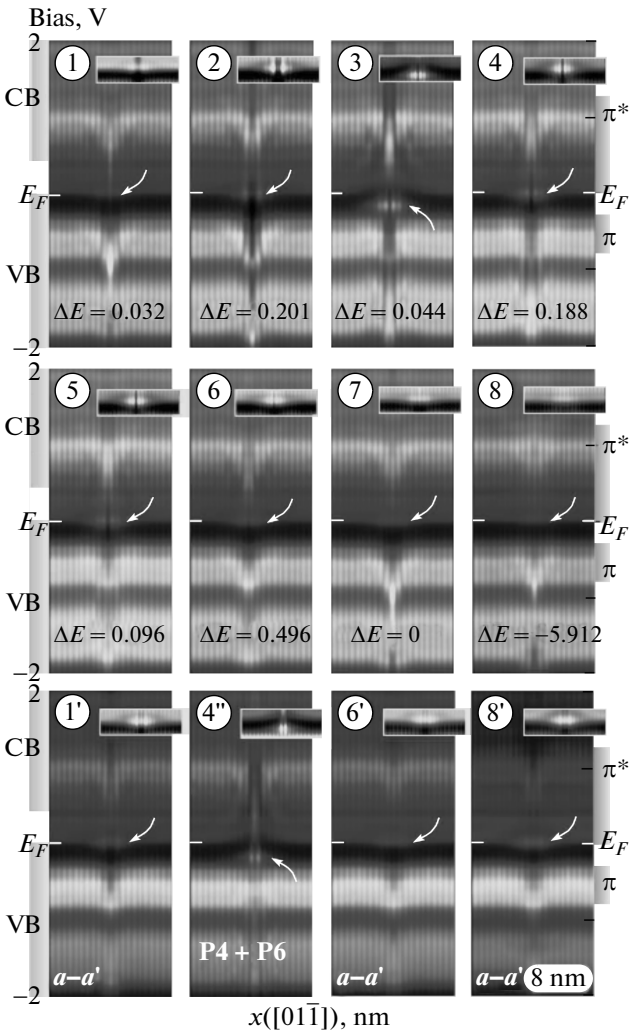

Fig. 8. (1–8) LDOS(x, eV) maps along the b–b' dimer row in the vicinity of a P atom located at different positions in subsurface layers of the Ge(111)-(2 × 1) surface. Numbers indicate the atom position (see Fig. 2). The energy difference ΔE in electronvolts relative to position 7 as well as the split-state position are indicated. The area of the split state is zoomed in on every panel. ($1'$, $6'$, $8'$) LDOS(x, eV) maps along the a–a' dimer row in the case where two π-bonded rows are disturbed by an impurity atom; ($4''$) LDOS(x, eV) map for two donor atoms located at positions 4 and 6. Note the split state located below the Fermi level

3.4. DFT surface LDOS around a P donor impurity

We note the most important features of the calculated images. As we have discussed earlier, the empty SS band π^* is governing the STM image formation for the Ge(111)-(2 × 1) surface [18, 23] in the band gap region. Now the same concerns the split state. The STM image is dominated by the split state in the vicinity of the Fermi energy. The noticeable influence of surface states inside the CB and VB can be inferred from Fig. 8. There are LDOS peculiarities near the top of the empty SS band π^* and at the edges of the filled SS band π. They are imaged as horizontal bright stripes. For all P doping atom positions except position 3, the split state is located at the Fermi level. When the P impurity is placed at position 3, the split state can be

observed below the Fermi energy (Fig. 8(3)). Position 2 is somewhat specific. In this case, the impurity atom is directly breaking the π-bonded chain, and this strongly influences $\mathrm{LDOS}(x, eV)$ (Fig. 8(2)): at almost all possible bias voltage values, the impurity LDOS image has two well-pronounced peaks.

As with other semiconductors, an individual impurity is visible in STM experiment when it is located below the Ge(111)-(2 × 1) surface (Fig. 8(5–8)).

To the best of our knowledge, we report this for the first time (albeit it should be rather obvious from simple speculations). The crystal lattice is disturbed noticeably far from an atomic-size defect [19], and this disturbs the perfectness of collective π-bonding in a few dimer rows. There is also another possibility. The P impurity is a shallow impurity in Ge, its ionization energy is 13 meV. Therefore, its localization radius should be large, in a 50 Å range. The LDOS observed by STM for the Ge(111)-(2×1) surface, in particular, must have two contributions: one quasi-1D, coming from surface reconstruction, and the other coming from ionized donors with large localization radii. These two contributions are superimposed on each other. The resulting STM image would be a linear structure caused by (2×1) reconstruction, with wide spots originating from impurities. These spots are poorly visible because of perfect screening by π-bonded electrons, but some influence should exist. The calculations for an impurity deep below the surface are to be done in the future and there is a need to reanalyze experimental data thinking in this direction.

We also mention that the above speculations must be taken with great care, because common sense might often be misleading in surface physics. The overall behavior of impurity LDOS images strongly differs, depending on the position of the donor atom in the crystal cell. This is observed even for subsurface defects. The same P donor impurity may looks as a protrusion, a depression, a protrusion superimposed on a depression, etc. It depends both on the spatial location of the impurity and on the applied bias voltage. The atomic orbitals in the vicinity of surface defects are strongly hybridized. This results in a bending of up/downward band edges. The insets in Fig. 8, with split state areas zoomed in with high contrast, illustrate this. Basically, the orbital hybridization leads to a specific spatial shape of the tunneling spectra $\mathrm{LDOS}(x, eV)$ and, in other words, to the appearance of local electronic density spatial oscillations [18, 19]. We note that these are not charge density oscillations, because they are observed in the empty-state energy range (above the Fermi level).

Spatial LDOS oscillations on the Ge(111)-(2 × 1) surface were the subject of Ref. [24]. The energy differences measured with respect to the total energy of the system of 2646 atoms with a P donor atom at position 7 are shown on every pane in Fig. 8. The difference is not very large. At least, we suppose, it does not allow making any conclusions about the most favorable position of the donor atom. The difference is large for donor positions 8. We do not have any explanation for the huge energy gain for impurity position 8. At the same time, this energy difference applies to a huge surface slab. Due to slightly different atom relaxation, a few electronvolts can easily be acquired by the whole supercell. Also, the thickness of the model slab might not be sufficient.

The last row in Fig. 8 is to be described in what follows. The LDOS (and STM) image of an individual impurity is dominated by the split state at zero (see Fig. 2) and the low bias (see above) voltage as illustrated by Fig. 9, where zero bias maps of $\mathrm{LDOS}(x, y)|_{eV=0}$ for different donor atom positions are presented together with the corresponding quasi-3D images. The profiles along the b–b' direction (the same for Fig. 2 and Fig. 9) are shown on the maps with equal scales.

Three things can be immediately noticed from Fig. 9. First, one or two π-bonded rows are affected by the donor impurity. Second, one or two local maxima are present on the profile. Third, the distance between maxima can be one or two dimers along the π-bonded row (the $[01\bar{1}]$ direction). This is shown in Fig. 9 by thin lines and arrows and is summarized in Table 1. Thus, the P donor impurity at position 1 is imaged as a two-row feature with two maxima in a row and the double dimer distance between the maxima. To be absolutely accurate, not two, but a few rows are affected by the impurity. The situation is the same as with the spatial extent of the LDOS image protrusion. One should either increase the contrast of images (see Fig. 9*c*) or use profiles in analysis (Fig. 9*b*). Reducing to two disturbed rows allows classifying LDOS images of the impurity located at different positions.

Now we can return to the lowest row in Fig. 8. Images $1'$, $6'$, and $8'$ correspond to cross sections of the $\mathrm{LDOS}(x, y, eV)$ scalar field along the (a–a') plane (see Fig. 2), i. e., along the second (along with b–b') disturbed π-bonded row. As can be seen from Fig. 8, the split state is also present on these images (see also Fig. 3). Images $6'$ and $8'$ are similar, with the main difference being the image contrast. The LDOS image for the P donor placed at position 7 is not shown because the LDOS maps along a–a' and b–b' dimer rows are al-

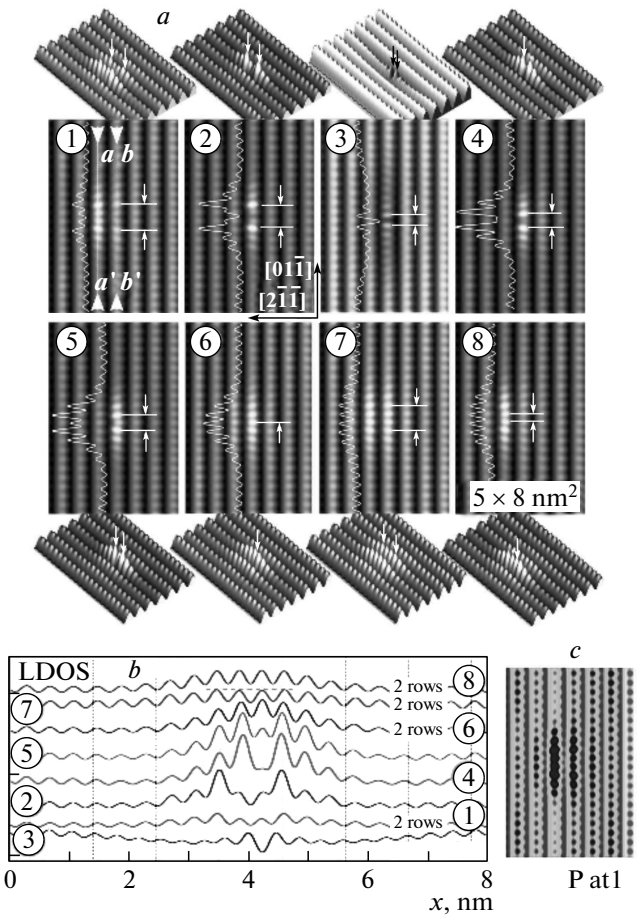

Fig. 9. (a) LDOS(x, y) maps in vicinity of a P atom located at different positions in subsurface layers of the Ge(111)-(2 × 1) surface. Numbers denote atom positions. Maps are given for a zero bias voltage. Profiles along the b–b' line are sketched on maps. White lines and arrows mark the positions of maxima in the dimer row nearest to the impurity atom. Crystallographic directions and image size are indicated. The lines a–a' and b–b' are the same as in Fig. 2. (b) The profiles of LDOS(x, y) maps along the b–b' line on the same scale. Note the shift of the profile for position 2. (c) High-contrast LDOS(x, y) map for the impurity at position 1, illustrating the disturbance of the surface electronic structure in a few π-bonded dimer rows

most identical. At the same time, in other cases, the difference between the a–a' and b–b' maps is rather big. The only exceptional case among LDOS(x, eV) images 1–8 is the case of the impurity at position 3, when the split state goes below the Fermi level.

To check whether this situation can be reproduced with a slightly different atomic environment, we have performed calculations for two impurities located at different positions in the atomic lattice. The first impurity was fixed at position 6, while the second was sequentially placed at positions from 1 to 4. The results for a P4–P6 pair are depicted in Fig. 8(4′). We can see that the split state for the impurity at position 4 was shifted below the Fermi level by adding the second impurity to position 6. Thus we proved that the split state location below the Fermi energy can be observed at different conditions. The comprehensive analysis of donor pairs is beyond the scope of this paper.

Table 1. P donor impurity LDOS image properties

Atom position	1	2	3	4	5	6	7	8
Two rows	+	−	−	−	−	+	+	+
Two maxima	+	+	+	+	+	−	+	+
Number of dimers	2	2	1	1	1	−	2	1

3.5. Spatial oscillations of LDOS

We have a data array with a high signal-to-noise ratio. Therefore, we can easily use some calibration scheme. Figure 10 depicts the ratio LDOS$(x, eV)/\langle$LDOS$(eV)\rangle_x$. The role of the split state becomes absolutely obvious. But we can also see hyperbolic branches. It is well known that such branches lead to the appearance of a quasilinear shape of the 1D Fourier spectrum. We can confirm this by detailed analysis of a single LDOS(x, eV) spectrum. This spectrum is a special case in the sense that it was calculated for a 35×7 surface slab to improve the quality of spectra. The 2D fast Fourier transform (FFT) spectrum is calculated by performing the 1D FFT on each row of the original image and then putting them next to each other. We can see the *sinc* envelope coming from a limited character of the 1D spectra and a bunch of quasi-1D disperging branches. These branches are located at higher harmonics of the main frequency. To show another method of obtaining hyperbolic branches, we can take the smoothed second spatial derivative $\delta(x)$, $\delta(eV)$. The result is shown on panel 3 in Fig. 11. This image has a close resemblance to the image in Fig. 10.

3.6. Model limitations

We specify the strong assumptions used in the present calculations. Some of them are imposed by the very big simulation supercell. In particular, we have

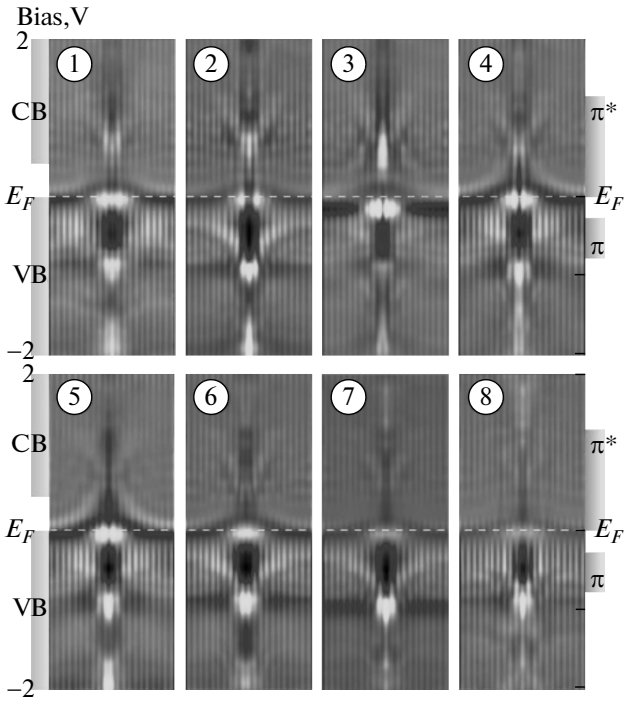

Fig. 10. Normalized LDOS$(x, eV)/\langle \text{LDOS}(eV)\rangle_x$ maps along the b–b' dimer row in the vicinity of the P atom located at different positions in subsurface layers of the Ge(111)-(2 × 1) surface. Numbers denote the atom position (see Fig. 2)

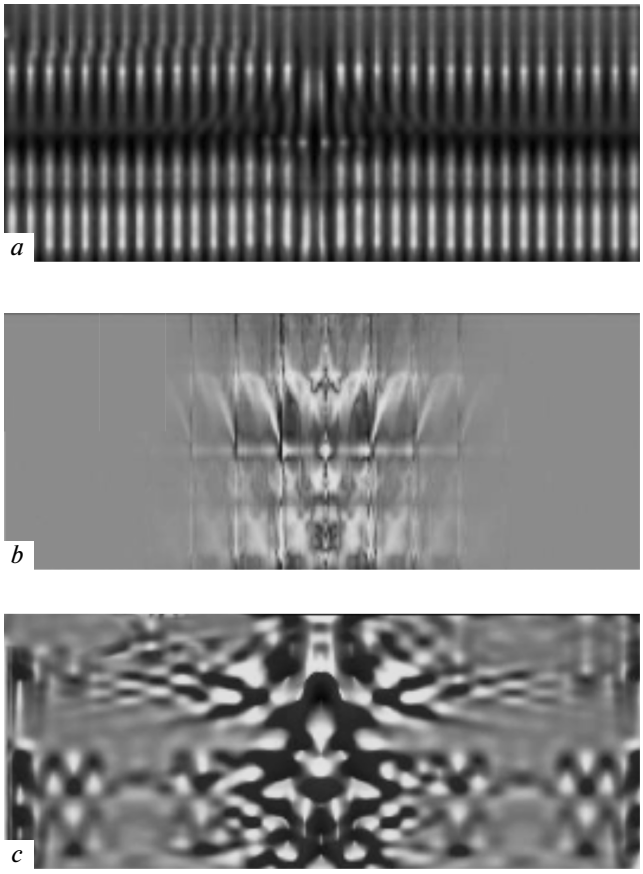

Fig. 11. (a) High-resolution LDOS(x, eV) image of a P impurity at position 3. (b) 2D FFT built from the 1D FFT of every row. (c) Smoothed second spatial derivative of LDOS(x, eV)

performed the simulation in the LDA approximation. It is known to give nonphysically small values of band gaps. This can be slightly improved by the general gradient approximation (GGA), but real improvements can be achieved only with computationally expensive GW many-body corrections [14]. At the same time, the cheap scissors method works quite well [3]. There is no STM tip density of states in our results. There is no correction for a closed STM feedback loop. The LDOS values are calculated on the plane above the surface. In our model, we cannot account for the surface band bending. We simply do not have a sufficiently thick model slab. Our slab is about 15 Å thick, and the depletion layer on the Ge(111)-(2 × 1) surface with the n type of bulk conductivity is almost 250 Å thick. The depletion layer strongly affects the picture of tunneling for n-type-doped Ge samples [8]. The same concerns the Si(111)-(2 × 1) surface. That is why our model STM images do not coincide exactly with experimental observations, but nevertheless the correspondence is reasonable. All LDOS(x, eV) maps (except at position 3) predict the presence of a protrusion on the STM images at a zero (and small) bias voltage, which indeed agrees with experiment. We did not find any substantial difference when explicitly adding charge to the impurity atom.

3.7. Low-temperature STM surface LDOS around the P donor impurity

Having the above classification, we can apply it to the test case. Si(111)-(2 × 1) and Ge(111)-(2 × 1) surfaces are similar in many senses. It is possible to perform a simple check of our results by comparing with the Si(111)-(2 × 1) surface [4]. In general, the situation with STM imaging of individual impurities is much simpler on the Si(111)-(2 × 1) surface. The empty SS band π^* and the VB are separated by a gap of about 0.4 eV [15]. Near the Fermi level, there are no states available for tunneling, but only empty surface states. That is why the STM impurity images on Si(111)-(2×1) are much easier to classify. In accordance with Fig. 9 and Table 1, the conclusions of the authors can be im-

Table 2. P donor impurity LDOS image properties

Atom position	1	2	3	4	5	6	7	8
Two rows	+	−	−	−	−	+	+	+
Two maxima	+	+	+	+	+	−	+	+
Number of dimers	2	2	1	1	1	−	2	1
Atom	c	a	g	d	e	f	b	h

mediately confirmed. In our notation, Fig. 2*a* in [4] corresponds to P in position 2, Fig. 2*b* in [4], to P in position 4, and Fig. 2*c* in [4], to P in position 1. The remaining unclear feature (Fig. 2*d* in [4]) most probably is the STM image of a vacancy at position 6.

We have also performed our own low-temperature STM investigation of a clean Ge(111) surface. The samples under investigation were cut from a heavily doped (resistivity 1 Ω·cm) Ge single crystal with n-type bulk conductivity. The doping element was phosphorus, which is a shallow impurity with the ionization energy 13 meV, and the doping ratio was rather high, about $8 \cdot 10^{18}$ cm^3. The samples were $1.5 \times 1.5 \times 5$ mm^3 slabs with the long axis aligned in the [111] direction. Samples were cleaved *in situ* in ultrahigh vacuum conditions and then immediately transfered to a low-temperature chamber with the base pressure $5 \cdot 10^{-12}$ Torr. The experiments have been done using the commercially available low-temperature UHV Omicron system. The system was equipped with a custom built sample cleavage mechanism. We have used tungsten tips sharpened with field emission.

Typical low-temperature STM images of the Ge(111)-(2 × 1) surface are presented in Fig. 12. The image in Fig. 12*a* depicts the domain boundary together with the impurity atom. With our simplified classification, we can state that it is a P atom at position 2: one row, two maxima, two dimer distance between maxima. Besides, it demonstrates excellent quality of images that are not filtered in any way. Using the same classification scheme, we arrive at Table 2, which is our main result. Our relatively simple model fits real world. Feature i does not correspond to an impurity located in the first two bilayers. We have also performed computer simulation for a vacancy located near the surface. The best correspondence between the STM image feature i is for a single atom vacancy located at site 6. Spatial oscillations around the impurity atom were observed experimentally [24].

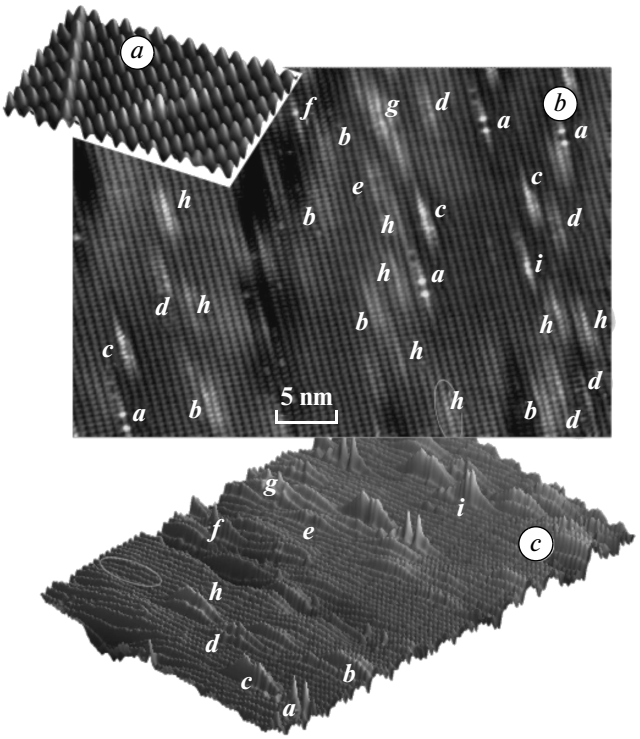

Fig. 12. (*a*) High-resolution STM image of a P impurity at position 2. (*b* and *c*) Two representations of the same surface area. Different features are marked by letters

4. CONCLUSION

In conclusion, we have performed a numerical modeling of the Ge(111)-(2 × 1) surface electronic properties in the vicinity of a P donor impurity atom located near the surface. We have found a notable increase in the surface LDOS around the surface dopant near the bottom of the empty surface-state band π^*, which we called the split state due to its limited spatial extent and energetic position inside the band gap. This state governs the STM image of an impurity in the vicinity of the Fermi energy on the Ge(111)-(2 × 1) surface. We show that despite the well-established bulk donor impurity energy level position at the very bottom of the conduction band, a surface donor impurity on the Ge(111)-(2 × 1) surface might produce an energy level below the Fermi energy, depending on the impurity atom local environment. It was demonstrated that the impurity located in subsurface atomic layers is visible in STM experiment on the Ge(111)-(2 × 1) surface. The quasi-1D character of the impurity image observed in STM experiments is confirmed by our computer simulations with a note

that a few π-bonded dimer rows may be affected by the presence of the impurity atom. We have elaborated a model that allows classifying atoms on an experimental low-temperature STM image. We showed the presence of spatial oscillations of the LDOS by DFT methods.

This work was supported by the RFBR (grant №13-02-01224a) and computing facilities of the Moscow State University. We also thank the authors of the WxSM and Chimera free software. One of the authors (C. v. H.) was supported by the Research Foundation Flanders (FWO, Belgium).

REFERENCES

1. M. Rohlfing, M. Palummo, G. Onida, and Del Sole, Phys. Rev. Lett. **85**, 5440 (2000).
2. A. A. Stekolnikov, J. Furthmüller, and F. Bechstedt, Phys. Rev. B **65**, 115318 (2002).
3. G. Bussetti, C. Goletti, P. Chiaradia et al., Surf. Sci. **602**, 1423 (2008).
4. J. K. Garleff, M. Wenderoth, R. G. Ulbrich et al., Phys. Rev. B **76**, 125322 (2007).
5. J. K. Garleff, M. Wenderoth, R. G. Ulbrich et al., Phys. Rev. B **72**, 073406 (2005).
6. T. Trappmann, C. Sürgers, and H. Löhneysen, Europhys. Lett. **38**, 177 (1997).
7. L. Oberbeck, N. Curson, T. Hallam et al., Thin Sol. Films **464–465**, 23 (2004).
8. P. I. Arseyev, N. S. Maslova, V. I. Panov et al., Pis'ma v Zh. Eksp. Teor. Fiz. **82**, 312 (2005) [JETP Lett. **82**, 279 (2005)].
9. M. Schöck, C. Sürgers, and H. v. Löhneysen, Phys. Rev. B **61**, 7622 (2000).
10. P. Studer, V. Brazdova, S. R. Schofield et al., ACS Nano **6**, 10456 (2012).
11. P. Studer, S. R. Schofield, C. F. Hirjibehedin, and N. J. Curson, Appl. Phys. Lett. **102**, 012107 (2013).
12. M. Koike, E. Shikoh, Y. Ando et al., Appl. Phys. Expr. **6**, 023011 (2013).
13. A. Jain, C. Vergnaud, J. Peiro et al., Appl. Phys. Lett. **101**, 022402 (2012).
14. C. Violante, A. Mosca Conte, F. Bechstedt, and O. Pulci, Phys. Rev. B **86**, 245313 (2012).
15. K. Löser, M. Wenderoth, T. K. A. Spaeth et al., Phys. Rev. B **86**, 085303 (2012).
16. G. Bussetti, B. Bonanni, S. Cirilli et al., Phys. Rev. Lett. **106**, 067601 (2011).
17. E. Artacho, D. Sanchez-Portal, P. Ordejon et al., Phys. Stat. Sol. (b) **215**, 809 (1999).
18. S. V. Savinov, S. I. Oreshkin, and N. S. Maslova, Pis'ma v Zh. Eksp. Teor. Fiz. **93**, 579 (2011) [JETP Lett. **93**, 521 (2011)].
19. S. V. Savinov, A. I. Oreshkin, and S. I. Oreshkin, Pis'ma v Zh. Eksp. Teor. Fiz. **96**, 33 (2012) [JETP Lett. **96**, 31 (2012)].
20. M. A. Olmstead and N. M. Amer, Phys. Rev. B **29**, 7048 (1984).
21. J. M. Nicholls, P. Märtensson, and G. V. Hansson, Phys. Rev. Lett. **54**, 2363 (1985).
22. P. I. Arseev, N. S. Maslova, V. I. Panov, and S. V. Savinov, Zh. Eksp. Teor. Fiz. **121**, 225 (2002) [JETP **94**, 191 (2002)].
23. P. I. Arseyev, N. S. Maslova, V. I. Panov et al., Pis'ma v Zh. Eksp. Teor. Fiz. **85**, 334 (2007) [JETP Lett. **85**, 277 (2007)].
24. D. A. Muzychenko, S. V. Savinov, V. N. Mantsevich et al., Phys. Rev. B **81**, 035313 (2010).